

Exceptional points and quantum dynamics in a non-Hermitian two-qubit system

Yi-Xi Zhang(张益玺), Zhen-Tao Zhang(张振涛), Zhen-Shan Yang(杨震山), Xiao-Zhi Wei(魏晓志), and Bao-Long Liang(梁宝龙)

Citation: Chin. Phys. B, 2024, 33 (**6**): 060308. DOI: 10.1088/1674-1056/ad2a70
Journal homepage: http://cpb.iphy.ac.cn; http://iopscience.iop.org/cpb

What follows is a list of articles you may be interested in

Anomalous time-reversal symmetric non-Hermitian systems

Yifei Yi(易益妃)
Chin. Phys. B, 2024, 33 (**6**): 060302. DOI: 10.1088/1674-1056/ad2502

Real eigenvalues determined by recursion of eigenstates

Tong Liu(刘通) and Youguo Wang(王友国)
Chin. Phys. B, 2024, 33 (**3**): 030303. DOI: 10.1088/1674-1056/ad1746

Hall conductance of a non-Hermitian two-band system with *k*-dependent decay rates

Junjie Wang(王俊杰), Fude Li(李福德), and Xuexi Yi(衣学喜)
Chin. Phys. B, 2023, 32 (**2**): 020305. DOI: 10.1088/1674-1056/ac9046

Characterizing entanglement in non-Hermitian chaotic systems via out-of-time ordered correlators

Kai-Qian Huang(黄恺芊), Wei-Lin Li(李蔚琳), Wen-Lei Zhao(赵文垒), and Zhi Li(李志)
Chin. Phys. B, 2022, 31 (**9**): 090301. DOI: 10.1088/1674-1056/ac67c3

Application of non-Hermitian Hamiltonian model in open quantum optical systems

Hong Wang(王虹), Yue Qin(秦悦), Jingxu Ma(马晶旭), Heng Shen(申恒), Ying Hu(胡颖), and Xiaojun Jia(贾晓军)
Chin. Phys. B, 2021, 30 (**5**): 050301. DOI: 10.1088/1674-1056/abda30

Exceptional points and quantum dynamics in a non-Hermitian two-qubit system

Yi-Xi Zhang(张益玺), Zhen-Tao Zhang(张振涛)†, Zhen-Shan Yang(杨震山)‡, Xiao-Zhi Wei(魏晓志), and Bao-Long Liang(梁宝龙)

School of Physics Science and Information Technology, Shandong Key Laboratory of Optical Communication Science and Technology, Liaocheng University, Liaocheng 252059, *China*

(Received 9 December 2023; revised manuscript received 29 January 2024; accepted manuscript online 19 February 2024)

We study the exceptional-point (EP) structure and the associated quantum dynamics in a system consisting of a non-Hermitian qubit and a Hermitian qubit. We find that the system possesses two sets of EPs, which divide the system-parameter space into $\mathcal{PT}$-symmetry unbroken, partially broken and fully broken regimes, each with distinct quantum-dynamics characteristics. Particularly, in the partially broken regime, while the $\mathcal{PT}$-symmetry is generally broken in the whole four-dimensional Hilbert space, it is preserved in a two-dimensional subspace such that the quantum dynamics in the subspace are similar to those in the $\mathcal{PT}$-symmetry unbroken regime. In addition, we reveal that the competition between the inter-qubit coupling and the intra-qubit driving gives rise to a complex pattern in the EP variation with system parameters.

Keywords: non-Hermitian system, exceptional point, $\mathcal{PT}$-symmetry

PACS: 03.65.–w, 03.65.Yz, 03.67.–a **DOI:** 10.1088/1674-1056/ad2a70

1. Introduction

Non-Hermitian quantum systems are currently a frontier research area in quantum physics.[1–8] Generally, a quantum system isolated from the external environment is governed by a Hermitian Hamiltonian. However, in practice, isolated systems are difficult to achieve and it is thus necessary to consider systems with dissipation, which could be effectively described by non-Hermitian Hamiltonians under proper circumstances. The Hamiltonian eigenvalues of a non-Hermitian system are generally complex and the eigenvectors might not be orthogonal,[9,10] which could yield novel characteristics and phenomena[11–14] that are absent in Hermitian systems.

Various mechanisms[15–24] exist for the realization of non-Hermitian quantum systems, which include introducing mode-selective loss, embedding the desired non-Hermitian subsystem within a larger Hermitian system or mitigating quantum jump events in a dissipative quantum system through measurement post-selection.[25–27] One of the most remarkable characteristics of the non-Hermitian system is the exceptional point (EP), at which not only some of the Hamiltonian eigenvalues, but also the corresponding eigenvectors, are degenerate.[28–30] Extraordinary effects emerge in the vicinity of an EP, such as loss-induced transparency,[31] unidirectional invisibility[32] and asymmetric mode conversion.[33,34] In addition, EPs can be exploited to manipulate the generation and stabilization of entanglement.[35–39] For example, in Ref. [38], the EP properties and entanglement dynamics are studied for a non-Hermitian system consisting of two identical qubits with balanced loss and gain and coupled via Ising-type interaction, which reveals steady-state entanglement in the $\mathcal{PT}$-symmetry broken regime and collapse-revival of entanglement in the $\mathcal{PT}$-symmetry unbroken regime, as well as speeding up of entanglement generation by virtue of the non-Hermiticity. Therefore, it is of great importance to explore the full EP structure and the associated dynamics in more diverse non-Hermitian quantum systems.[40–42]

In this paper, we conduct an in-depth study of the EPs and the associated dynamic characteristics of a quantum system consisting of a Hermitian qubit and a non-Hermitian qubit[43,44] that are transversely coupled to each other. We find two sets of EPs, which divide the parameter space into 3 distinct regions, respectively, corresponding to the $\mathcal{PT}$-symmetry[45–50] unbroken, partially broken and fully broken regimes: (1) in the $\mathcal{PT}$-symmetry unbroken regime, all the Hamiltonian eigenvalues have exactly the same imaginary part; (2) in the opposite $\mathcal{PT}$-symmetry fully broken regime, all the eigenvalues have different imaginary parts; (3) in the intermediate $\mathcal{PT}$-symmetry partially broken regime, two (and only two) of the eigenvalues have an identical imaginary part, which suggests that the $\mathcal{PT}$-symmetry, while broken in the whole four-dimensional Hilbert space, is nonetheless preserved in the two-dimensional subspace spanned by the two eigenvectors corresponding to the eigenvalues with the same imaginary part. Also, the real parts of the eigenvalues possess structural features that are distinct in different $\mathcal{PT}$-symmetry regimes. We show that the quantum dynamics characteristics are qualitatively different in the $\mathcal{PT}$-symmetry unbroken, partially broken and fully broken regimes, with the imaginary

†Corresponding author. E-mail: zhzhentao@163.com
‡Corresponding author. E-mail: yangzhenshan@lcu.edu.cn

© 2024 Chinese Physical Society and IOP Publishing Ltd

parts of the eigenvalues essentially determining whether the system would evolve into a steady state and the real parts determining the transient-process behaviors in the evolution. Furthermore, we investigate the impact of the inter-qubit coupling on the EP structure and reveal that a weak inter-qubit coupling would split the third-order EP in the originally uncoupled two-qubit system into two second-order EPs, and as the inter-qubit coupling is far stronger than the intra-qubit driving, the EPs are essentially determined by the coupling. In the intermediate region where the coupling is comparable to the driving, the competition between the two impacts gives rise to a complex pattern in the EP variation with system parameters.

The paper is organized as follows. In Section 2, we present the model and the Hamiltonian for the non-Hermitian coupled two-qubit system. In Section 3, we analyze the EP structure and the associated $\mathcal{PT}$-symmetry regimes of the system consisting of a Hermitian qubit and a non-Hermitian qubit. In Section 4, we study the quantum dynamics characteristics in the distinct $\mathcal{PT}$-symmetry regimes. In Section 5, the impact of the inter-qubit coupling on the EP structure is investigated. A summary of our main results is given in Section 6.

2. Non-Hermitian coupled two-qubit system: Model and Hamiltonian

The coupled non-Hermitian two-qubit system under consideration is shown in Fig. 1. Both of the qubits contain two free energy levels $|f_\mu\rangle$ and $|e_\mu\rangle$, with $\mu = 1,2$ labeling qubits 1 and 2, respectively. Each qubit can be regarded as a two-dimensional subspace of a qutrit with 3 free energy levels $|f\rangle$, $|e\rangle$ and $|g\rangle$, where coherent transitions between $|f\rangle$ and $|e\rangle$ are allowed under external driving, and incoherent transition from $|e\rangle$ to $|g\rangle$ occurs due to, e.g., spontaneous emission. By monitoring whether or not the qutrit is in state $|g\rangle$ and selecting only the "no" events,[51] the two-dimensional subspace spanned by $\{|f\rangle, |e\rangle\}$ can be treated as a qubit system governed by a non-Hermitian Hamiltonian. Without inter-qubit coupling, the Hamiltonian for qubit μ can be written as ($\hbar = 1$)[37]

$$\bar{H}_{\mu 0} = \left(\Delta_\mu - \frac{\mathrm{i}\gamma_\mu}{2}\right)|e_\mu\rangle\langle e_\mu| + \Omega_\mu\left(|e_\mu\rangle\langle f_\mu| + |f_\mu\rangle\langle e_\mu|\right), \quad (1)$$

where $\gamma_\mu \geq 0$ denotes the dissipation rate from $|e_\mu\rangle$ to $|g_\mu\rangle$, Ω_μ and Δ_μ represent the strength and detuning of the external driving for the transition between $|e_\mu\rangle$ and $|f_\mu\rangle$. As the two qubits are coupled transversely, the total Hamiltonian reads

$$\bar{H} = \sum_{\mu=1,2}\bar{H}_{\mu_0} + J\left(|f_1 e_2\rangle\langle e_1 f_2| + |e_1 f_2\rangle\langle f_1 e_2|\right), \quad (2)$$

with J being the strength of the inter-qubit coupling. Note that in Eqs. (1) and (2), for simplicity but without loss of generality, we have assumed Ω_μ and J to be real and non-negative. In the experiment, following the idea in Ref. [51], we can implement the qutrits using the lowest energy levels $|g\rangle$, $|e\rangle$ and $|f\rangle$ of a transmon superconducting circuit in a three-dimensional copper microwave cavity. The decay rates from $|f\rangle \to |e\rangle$ (κ) and $|e\rangle \to |g\rangle$ (γ) are controlled by mediating the interaction between the circuit and the cavity electromagnetic field of a non-uniform density of states (in our current work, the decay rates should be tuned to guarantee that $\kappa \ll \gamma$ and thus κ can be ignored). Also, as mentioned above, the ground state $|g\rangle$ can be used to monitor the quantum jumps from $|e\rangle$, with post-selection being performed such that the subspace spanned by $\{|e\rangle, |f\rangle\}$ is effectively governed by the non-Hermitian Hamiltonian.

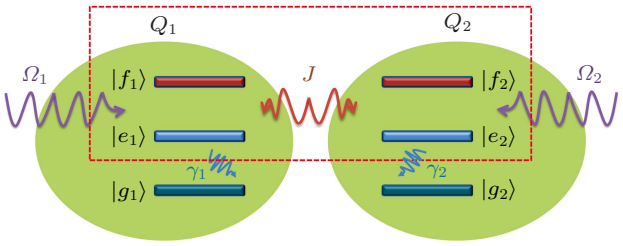


Fig. 1. Schematic of a non-Hermitian coupled two-qubit system (inside the red rectangular frame). Each qubit ($\{|f_\mu\rangle, |e_\mu\rangle\}$) can be regarded as the two-dimensional subspace of a qutrit ($\{|f_\mu\rangle, |e_\mu\rangle, |g_\mu\rangle\}$, with an incoherent transition rate γ_μ from $|e_\mu\rangle$ to $|g_\mu\rangle$). The qubits are subject to intra-qubit driving Ω_μ and inter-qubit coupling J. With $\gamma_1 \neq 0$ and $\gamma_2 = 0$, qubit 1 is non-Hermitian and qubit 2 is Hermitian.

The two-qubit system evolves according to the Schrödinger equation

$$\mathrm{i}\hbar\frac{\mathrm{d}}{\mathrm{d}t}|\psi(t)\rangle = \bar{H}|\psi(t)\rangle. \quad (3)$$

Due to the non-Hermiticity of the Hamiltonian, the evolution is non-unitary and thus $|\psi(t)\rangle$ might become unnormalized. In accordance with the probability interpretation of quantum mechanics, $\langle\psi(t)|\psi(t)\rangle$ would represent the probability of finding at time t the originally two-qutrit system to remain in the two-qubit subspace spanned by $\{|f_1 f_2\rangle, |f_1 e_2\rangle, |e_1 f_2\rangle, |e_1 e_2\rangle\}$ (i.e., neither of the qutrits decaying into $|g_\mu\rangle$). The quantum state at time t can be normalized as

$$\begin{aligned}|\tilde{\psi}(t)\rangle &= \frac{|\psi(t)\rangle}{\sqrt{\langle\psi(t)|\psi(t)\rangle}} \\ &= \alpha|f_1 f_2\rangle + \beta|f_1 e_2\rangle + \varepsilon|e_1 f_2\rangle + \zeta|e_1 e_2\rangle, \end{aligned} \quad (4)$$

where $|\alpha|^2 + |\beta|^2 + |\varepsilon|^2 + |\zeta|^2 = 1$.

In this paper, we are interested in a coupled two-qubit system consisting of a non-Hermitian qubit (qubit 1) and a Hermitian qubit (qubit 2, $\gamma_2 = 0$), with $\Omega_1 = \Omega_2 = \Omega$. Also, in numerical simulations, it is necessary to deal with dimensionless quantities. Therefore, we first convert γ, J, Ω and t to dimensionless $\gamma' \equiv \gamma/\Omega$, $J' \equiv J/\Omega$, $\Omega' \equiv \Omega/\Omega = 1$, $t' \equiv t/\Omega^{-1}$, and after numerically solving all the equations, we again convert the dimensionless quantities back to their counterparts with actual units.

3. Exceptional points and $\mathcal{PT}$-symmetry regimes

In a non-Hermitian quantum system, EPs typically serve as "phase transition" boundaries in the system-parameter space, with different "phase" regimes manifesting qualitatively different quantum dynamics. Both the EPs and the quantum dynamics are closely related to the eigenvalues and eigenvectors of the non-Hermitian Hamiltonian. In this section, by calculating the Hamiltonian eigenvectors and eigenvalues, we investigate the EP structure and the associated "phase" regimes of the non-Hermitian coupled two-qubit system illustrated in Section 2, while the quantum dynamics in different "phase" regimes will be studied in Section 4. The system (non-Hermitian qubit 1 + Hermitian qubit 2) parameters are the coupling strength J, the driving amplitude Ω and the dissipation rate $\gamma_1 \equiv \gamma$ of qubit 1.

In our analysis, we set the inter-qubit coupling strength $J = 1$ rad/μs and the intra-qubit driving amplitude $\Omega = 2$ rad/μs. The dissipation rate γ varies from 0 to 15 μs^{-1} and we calculate the Hamiltonian eigenvalues and eigenvectors for each γ. By checking the number of linearly independent eigenvectors, we find that $\gamma = 6$ μs^{-1} and $\gamma = 10$ μs^{-1} are second-order EPs, i.e., at each of the γ's, two of the Hamiltonian eigenvectors coalesce and thus $M_e = M_H - 1$, with M_e being the number of linearly independent eigenvectors and M_H the dimension of the Hilbert space. For later convenience, we designate the EPs as EP1 ($\gamma = 6$ μs^{-1}) and EP2 ($\gamma = 10$ μs^{-1}).

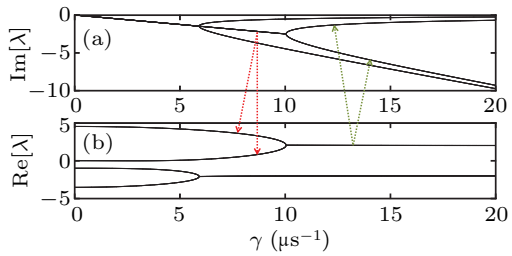


Fig. 2. Imaginary parts (a) and real parts (b) of the non-Hermitian Hamiltonian eigenvalues as functions of γ, with $J = 1$ rad/μs and $\Omega = 2$ rad/μs. The arrows serve to clarify the correspondence between the real and imaginary parts of the eigenvalues.

The real and imaginary parts of the Hamiltonian eigenvalues, as functions of γ, are plotted in Fig. 2, which shows that the two EPs divide the γ-parameter axis into three regions. To the left of EP1 ($\gamma < 6$ μs^{-1}), the imaginary parts [Fig. 2(a)] of the Hamiltonian eigenvalues are all identical and thus the system possesses $\mathcal{PT}$-symmetry. In the middle of the two EPs (6 $\mu s^{-1} < \gamma < 10$ μs^{-1}), only two of the imaginary parts are identical, which suggests that the $\mathcal{PT}$-symmetry is partially broken. More precisely, although the $\mathcal{PT}$-symmetry is broken in the four-dimensional Hilbert space of the two-qubit system, it is preserved in the two-dimensional subspace spanned by the two eigenvectors that correspond to the eigenvalues with identical imaginary parts. To the right of EP2 ($\gamma > 10$ μs^{-1}), all eigenvalues of the Hamiltonian have different imaginary parts, clearly indicating a full breakdown of the $\mathcal{PT}$-symmetry. Therefore, there are three distinct "phase" regimes of the system, i.e., the $\mathcal{PT}$-symmetry unbroken, partially broken and fully broken regimes, which are separated by the two EPs. As will be discussed in Section 4, the different $\mathcal{PT}$-symmetry regimes display qualitatively different quantum-dynamics characteristics.

As will become clear in Section 4, the imaginary parts of the Hamiltonian eigenvalues essentially determine whether the system would evolve into a steady state. On the other hand, the real parts of the Hamiltonian eigenvalues mainly determine the transient dynamics of the system. Therefore, it is also of interest to look into the real-part eigenvalue structure in the different $\mathcal{PT}$-symmetry regimes, as illustrated in Fig. 2(b). We can see that: (1) in the $\mathcal{PT}$-symmetry unbroken regime, all of the four eigenvalues have distinct real parts (and identical imaginary parts); (2) in the $\mathcal{PT}$-symmetry partially broken regime, two of the eigenvalues have identical real parts (and distinct imaginary parts), while the other two eigenvalues have distinct real parts (and identical imaginary parts); (3) in the $\mathcal{PT}$-symmetry fully broken regime, the two eigenvalues with distinct real parts in the "partially broken" regime now also have identical real parts (but distinct imaginary parts), and thus there are only two distinct real parts (but four distinct imaginary parts) for the Hamiltonian eigenvalues. The effects of the real-part structure on the transient behaviors of the quantum dynamics will be detailed in Section 4.

The above analysis is for a simple one-dimensional parameter (γ) axis. To gain a deeper insight, we calculate the EPs in the two-dimensional parameter (Ω–γ) plane (with $J = 1$ rad/μs) and plot the results as a "phase" diagram in Fig. 3. There are two EP curves, which divide the Ω–γ plane into 3 regions, respectively, corresponding to the $\mathcal{PT}$-symmetry unbroken (lower region, green), partially broken (middle region, blue) and fully broken (upper region, yellow) regimes.

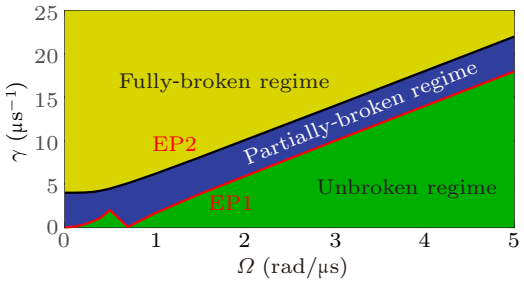


Fig. 3. Diagram of EP curves and associated $\mathcal{PT}$-symmetry regimes in the Ω–γ plane, with $J = 1$ rad/μs.

The mechanism for the existence of two sets of EPs can be explained as follows. For a given Ω, without inter-qubit coupling J, the Hermitian qubit (qubit 2) possesses no EP and thus always has two orthogonal Hamiltonian eigenvectors with eigenvalues $\pm\Omega$; on the other hand, the non-Hermitian qubit

(qubit 1) possesses one EP at $\gamma = 4\Omega$ and the non-Hermitian Hamiltonian has only one eigenvector with eigenvalue $-\mathrm{i}\gamma/4$. As a composite four-dimensional system, the uncoupled two qubits have one third-order EP at $\gamma = 4\Omega$, with only two linearly independent eigenvectors (thus $M_{\mathrm{e}} = M_{\mathrm{H}} - 2$), respectively corresponding to eigenvalues $\pm\Omega - \mathrm{i}\Omega$. Now, if we impose the inter-qubit coupling J, the eigenvector degeneracy in the third-order EP would be partially lifted and the third-order EP would split into two second-order EPs, as observed in Figs. 2 and 3. More detailed relations between the EPs and the inter-qubit coupling will be discussed in Section 5.

4. Quantum dynamics in different $\mathcal{PT}$-symmetry regimes

The $\mathcal{PT}$-symmetry regimes associated with the EPs are closely related to the quantum dynamics characteristics of the system. In this section, we analyze and compare the quantum dynamics in the distinct regimes.

The quantum dynamics of the system are determined by the Hamiltonian eigenvalues and eigenvectors (except at the EPs), as follows. The initial state of the system can be decomposed into a linear superposition of the Hamiltonian eigenvectors

$$|\psi(t=0)\rangle = \sum_{n=1}^{4} c_n |\lambda_n\rangle, \tag{5}$$

where $|\lambda_n\rangle$ are the eigenvectors with λ_n as the corresponding complex eigenvalues. According to the Schrödinger equation, the quantum state evolves as

$$|\psi(t)\rangle = \sum_{n=1}^{4} c_n \exp\{\mathrm{Im}(\lambda_n)t - \mathrm{iRe}(\lambda_n)t\} |\lambda_n\rangle. \tag{6}$$

If the imaginary parts $\mathrm{Im}(\lambda_n)$ for non-zero c_n's in the expansion of $|\psi(t)\rangle$ are not all identical, then at sufficiently large t only the eigenstate ($|\lambda_n^{(\mathrm{min})}\rangle$) with the minimum $|\mathrm{Im}(\lambda_n)|$ would survive after the normalization of $|\psi(t)\rangle$ (all other $|\lambda_n\rangle$ components would decay to zero), which means that the system would eventually settle into the steady state $|\lambda_n^{(\mathrm{min})}\rangle$. On the other hand, if all $\mathrm{Im}(\lambda_n)$ for non-zero c_n's are identical in Eq. (6), then no components of $|\psi(t)\rangle$ would decay after normalization and the system would typically not reach a steady state. Therefore, the imaginary parts of the Hamiltonian eigenvalues essentially determine the steady-state dynamics characteristics, i.e., whether or not the system would evolve into a steady state and, if it does, into which steady state.

Furthermore, the real parts of the Hamiltonian eigenvalues would basically determine the transient behaviors in the quantum dynamics, since the real parts would yield time-dependent phase differences among the $|\lambda_n\rangle$ components of $|\psi(t)\rangle$. Qualitatively, each time-dependent phase difference between two components $|\lambda_m\rangle$ and $|\lambda_{m'}\rangle$ would contribute a beat of frequency $\Delta\omega = |\mathrm{Re}(\lambda_m) - \mathrm{Re}(\lambda_{m'})|$ (or period of $2\pi/\Delta\omega$) in the state evolution, and there might exist more than one beat if more than two distinct real-part values exist in the expansion of $|\psi(t)\rangle$.

Based on the above mechanisms, we now investigate the quantum dynamics in the three distinct $\mathcal{PT}$-symmetry regimes. In Fig. 4, we show the evolution of the populations in the free basis $\{|f_1 f_2\rangle, |f_1 e_2\rangle, |e_1 f_2\rangle, |e_1 e_2\rangle\}$. With the system initially in $|f_1 f_2\rangle$, the dynamics of the system are plotted for $\gamma = 2\ \mu\mathrm{s}^{-1}$ ($\mathcal{PT}$-symmetry unbroken), $\gamma = 8\ \mu\mathrm{s}^{-1}$ ($\mathcal{PT}$-symmetry partially broken) and $\gamma = 11\ \mu\mathrm{s}^{-1}$ ($\mathcal{PT}$-symmetry fully broken) as the red-solid, blue-dash-dot, and black-dashed curves. One can see that in the $\mathcal{PT}$-symmetry unbroken regime, the state keeps oscillating with no sign of stabilization, while in both the partially broken and fully broken regimes, the system eventually settles into a steady state. The results are consistent with the fact that the imaginary parts of the Hamiltonian eigenvalues are all identical in the $\mathcal{PT}$-symmetry unbroken regime, but not in the partially broken or fully broken regimes.

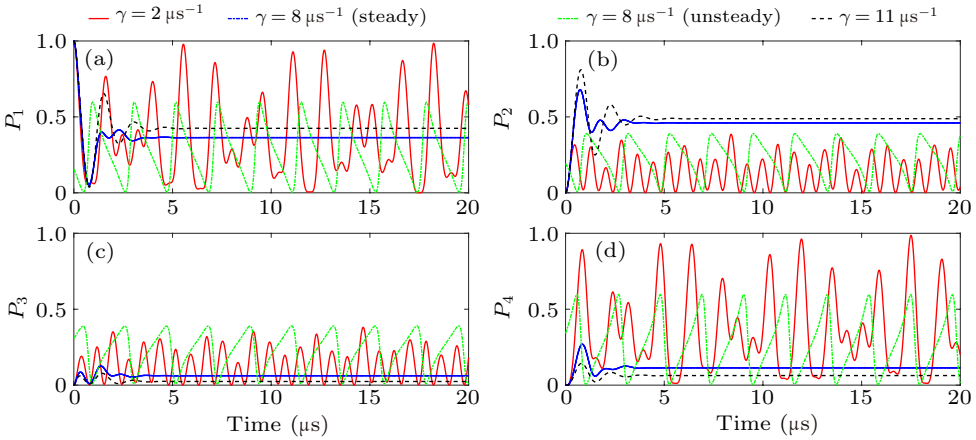


Fig. 4. With $J = 1$ rad/μs, $\Omega = 2$ rad/μs and various γ, evolution of populations of $|f_1 f_2\rangle$ (P_1), $|f_1 e_2\rangle$ (P_2), $|e_1 f_2\rangle$ (P_3), and $|e_1 e_2\rangle$ (P_4) are plotted in (a), (b), (c) and (d), respectively. The correspondence between the γ values and the $\mathcal{PT}$-symmetry regimes are $\gamma = 2\ \mu\mathrm{s}^{-1}$ (unbroken), $\gamma = 8\ \mu\mathrm{s}^{-1}$ (partially broken) and $\gamma = 11\ \mu\mathrm{s}^{-1}$ (fully broken). For $\gamma = 2\ \mu\mathrm{s}^{-1}$, $\gamma = 8\ \mu\mathrm{s}^{-1}$ (steady) and $\gamma = 11\ \mu\mathrm{s}^{-1}$, the initial state is $|f_1 f_2\rangle$, and for $\gamma = 8\ \mu\mathrm{s}^{-1}$ (unsteady), the initial state is given in Eqs. (8) and (9).

Moreover, for the transient (i.e., unsteady) part of the evolution, in the unbroken (red-solid) and partially broken (blue-dash-dot) regimes, multiple-beat patterns can be observed, while in the fully broken regime (black-dashed) we only observe the one-beat pattern. This is also consistent with the real-part eigenvalue structure in the $\mathcal{PT}$-symmetry regimes: in the unbroken and partially broken regimes, there are more than two distinct real parts of the eigenvalues, which can lead to more than one beat in the transient dynamics; in the fully broken regime, there are only two distinct real parts, and thus the transient dynamics have only one beat in the pattern.

In the $\mathcal{PT}$-symmetry partially-broken regime, the initial state $|f_1 f_2\rangle$ eventually evolves into a steady state (blue-dash-dot curve in Fig. 4) because $|\psi(t)\rangle$ [Eq. (6)] contains eigenvector components with different $|\mathrm{Im}(\lambda_n)|$. The system eventually settles into the eigenvector with the minimum $|\mathrm{Im}(\lambda_n)|$. However, in the two-dimensional subspace (named the $\mathcal{PT}$ subspace for convenience) spanned by the two eigenvectors that correspond to the eigenvalues with identical imaginary parts [Fig. 2(a)], the $\mathcal{PT}$-symmetry is unbroken. Therefore, if the initial state is a superposition of the two eigenvectors in the $\mathcal{PT}$ subspace, then neither of the eigenvector components in $|\psi(t)\rangle$ would decay to zero after normalization. Furthermore, due to the distinct real parts of the two eigenvalues, the state would oscillate for all time. As an example, we set the initial state as

$$|\psi(0)\rangle = \frac{1}{\sqrt{2}}|\lambda_+\rangle + \frac{1}{\sqrt{2}}|\lambda_-\rangle, \tag{7}$$

where

$$\begin{aligned} |\lambda_+\rangle &= (0.28+0.38\mathrm{i})|f_1 f_2\rangle + (0.36+0.39\mathrm{i})|f_1 e_2\rangle \\ &\quad + 0.53|e_1 f_2\rangle + (0.47-0.05\mathrm{i})|e_1 e_2\rangle, \end{aligned} \tag{8}$$

$$\begin{aligned} |\lambda_-\rangle &= (-0.46+0.29\mathrm{i})|f_1 f_2\rangle + (-0.27+0.37\mathrm{i})|f_1 e_2\rangle \\ &\quad + (0.42+0.17\mathrm{i})|e_1 f_2\rangle + 0.54|e_1 e_2\rangle \end{aligned} \tag{9}$$

are the two normalized eigenvectors in the $\mathcal{PT}$ subspace. The state evolution is illustrated in Fig. 4 as the green-dash-dot curves, which clearly show that the state does not become steady, consistent with the preservation of $\mathcal{PT}$-symmetry in the subspace.

One of the most important quantum properties of a two-qubit system is the entanglement, which can be measured by the "concurrence" $\mathcal{C}$,[52–54]

$$\mathcal{C} = 2|\alpha\zeta - \beta\varepsilon|, \tag{10}$$

where α, β, ζ and ε are the coefficients in the normalized state $|\tilde{\psi}(t)\rangle$ [see Eq. (4)]. With the same initial states and system parameters as in Fig. 4, we plot the evolution of entanglement in Fig. 5. It is easy to understand that the steady-state characteristics and the transient behaviors in the entanglement evolution essentially reflect the corresponding features in the quantum-state evolution (in Fig. 4).

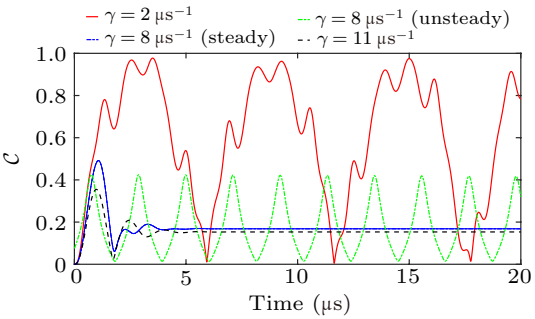


Fig. 5. Evolution of concurrence $\mathcal{C}$, with the same system parameters and initial states as in Fig. 4. The correspondence between the color–line style of the curves and the system parameter/initial state is also identical to that in Fig. 4.

5. Impact of inter-qubit coupling on EPs

The inter-qubit coupling plays an important role in the EP structure of the non-Hermitian two-qubit system. In the current section, we quantitatively investigate the impact of the coupling on the EP characteristics.

In an un-coupled system ($J = 0$), qubit 2 is Hermitian and has two orthogonal Hamiltonian eigenvectors $\frac{1}{\sqrt{2}}(|f_2\rangle \pm |e_2\rangle)$ with the corresponding eigenvalues of $\pm\Omega$, while qubit 1 is non-Hermitian and has two non-orthogonal Hamiltonian eigenvectors with eigenvalues $\lambda_\pm = \frac{1}{4}\left(-\mathrm{i}\gamma \pm \sqrt{16\Omega^2 - \gamma^2}\right)$. For qubit 1, if $\gamma = 4\Omega$, then the two eigenvalues, as well as the eigenvectors, are degenerate, i.e., the qubit is at the EP and has only one eigenvalue $-\mathrm{i}\Omega$ and one eigenvector $\frac{1}{\sqrt{2}}(|f_1\rangle - \mathrm{i}|e_1\rangle)$. Therefore, with $\gamma = 4\Omega$, the un-coupled two-qubit system (a four-dimensional Hilbert space) has only two linearly independent Hamiltonian eigenvectors $\frac{1}{2}(|f_1\rangle - \mathrm{i}|e_1\rangle) \otimes (|f_2\rangle \pm |e_2\rangle)$, and the system is at a third-order EP. Intuitively, as the inter-qubit coupling ($J > 0$) is imposed on the two-qubit system, the degeneracy in the eigenvalues and eigenvectors would be (at least partially) lifted and the third-order EP could split into two lower-order EPs.

To verify this, setting $\Omega = 1$ rad/μs we calculate the EPs in the J–γ plane and plot the results as the two curves in Fig. 6. It is clear that at $J = 0$ only one EP exists ($\gamma = 4$ rad/μs $= 4\Omega$), and with $J > 0$, the EP "splits" into two distinct points, thus yielding two distinct EP curves in the J–γ plane as J increases. This is fully consistent with the analysis in the previous paragraph.

For $J \gg \Omega$, we find that the γ on the upper EP curve approaches $4J$ and the γ on the lower curve tends to 0, which can be understood as follows. We first write the Hamiltonian (2) as a matrix in the basis $\{|f_1 f_2\rangle, |f_1 e_2\rangle, |e_1 f_2\rangle, |e_1 e_2\rangle\}$ (noting $\Omega_1 = \Omega_2 \equiv \Omega$, $\gamma_1 \equiv \gamma$ and $\gamma_2 = 0$)

$$\bar{H} = \begin{bmatrix} 0 & \Omega & \Omega & 0 \\ \Omega & 0 & J & \Omega \\ \Omega & J & -\frac{\mathrm{i}\gamma}{2} & \Omega \\ 0 & \Omega & \Omega & -\frac{\mathrm{i}\gamma}{2} \end{bmatrix}. \tag{11}$$

With $J \gg \Omega$, the Hamiltonian can be approximated as

$$\bar{H}_{J\gg\Omega} = \begin{bmatrix} 0 & 0 & 0 & 0 \\ 0 & 0 & J & 0 \\ 0 & J & -\frac{i\gamma}{2} & 0 \\ 0 & 0 & 0 & -\frac{i\gamma}{2} \end{bmatrix}, \tag{12}$$

which is actually a direct sum of two 2×2 matrices in the separate subspaces spanned by $\{|f_1e_2\rangle, |e_1f_2\rangle\}$ and $\{|f_1f_2\rangle, |e_1e_2\rangle\}$, respectively. In the $\{|f_1e_2\rangle, |e_1f_2\rangle\}$ subspace, the matrix is

$$\begin{pmatrix} 0 & J \\ J & -\frac{i\gamma}{2} \end{pmatrix}, \tag{13}$$

which possesses an EP at $\gamma = 4J$. In the $\{|f_1f_2\rangle, |e_1e_2\rangle\}$ subspace, the matrix is

$$\begin{pmatrix} 0 & 0 \\ 0 & -\frac{i\gamma}{2} \end{pmatrix}, \tag{14}$$

with the EP being at $\gamma \to 0$.

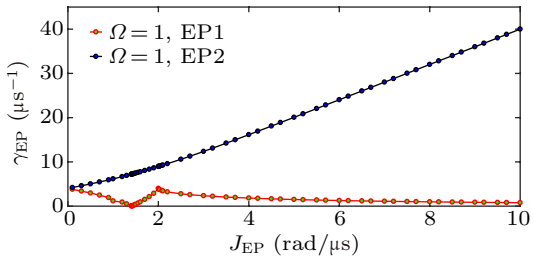


Fig. 6. Diagram of EP curves and associated $\mathcal{PT}$-symmetry regimes in the J–γ plane, with $\Omega = 1$ rad/μs.

In the intermediate region between $J \approx 0$ and $J \gg \Omega$, the EP variation with the coupling is complex, and two sets of EPs behave in qualitatively different characteristics. For the upper EP curve, γ increases monotonically with J, from $\gamma \approx 4\Omega$ at $J \approx 0$, to $\gamma \approx 4J$ at $J \gg \Omega$. In contrast, for the lower EP curve, γ first decreases with J until reaching $\gamma \approx 0$ at $J \approx 1.4\Omega$; then γ goes up as J further increases, reaching a maximum value of $\gamma \approx 4\Omega$ at $J \approx 2\Omega$; after that, γ monotonically decreases with J and tends to 0 at $J \gg \Omega$. The unusual behaviors of the EPs can be attributed to the competition between the impacts of the driving (Ω) and the coupling (J).

6. Conclusion

We have studied the EP structure and the associated dynamic characteristics in a quantum system consisting of a non-Hermitian qubit and a Hermitian qubit. We found that the system possesses two sets of EPs, which divide the system-parameter space into 3 distinct $\mathcal{PT}$-symmetry regimes, i.e., the $\mathcal{PT}$-symmetry unbroken, partially broken and fully broken regimes. Each $\mathcal{PT}$-symmetry regime manifests quantum dynamics qualitatively different from those in the other regimes. The quantum dynamics characteristics are closely related to the structural features of the eigenvalues, with the imaginary parts determining whether the system can evolve into a steady state and the real parts determining the transient behaviors of the quantum dynamics. Particularly, we showed that in the partially broken regime, while the $\mathcal{PT}$-symmetry is generally broken in the whole four-dimensional Hilbert space, it is preserved in a two-dimensional subspace such that the quantum dynamics in the two-dimensional subspace is similar to that in the $\mathcal{PT}$-symmetry unbroken regime. By further analyzing the impact of the inter-qubit coupling on the EP structure, we revealed that a weak inter-qubit coupling would split a third-order EP in the originally uncoupled two-qubit system into the two second-order EPs and a sufficiently strong coupling would overwhelm the intra-qubit driving in determining the EP structure; while in the intermediate region, the competition between the coupling and the driving leads to a complex pattern in the EP variation with system parameters. Our work can be helpful in the control of quantum dynamics by exploiting the non-Hermiticity of the system.

Acknowledgements

This work is partly funded by the Natural Science Foundation of Shandong Province of China (Grant Nos. ZR2021MA091 and ZR2018MA044), Introduction and Cultivation Plan of Youth Innovation Talents for Universities of Shandong Province (Research and Innovation Team on Materials Modification and Optoelectronic Devices at extreme conditions).

References

[1] Konotop V V, Yang J and Zezyulin D A 2016 *Rev. Mod. Phys.* **88** 035002
[2] Longhi S 2017 *Phys. Rev. A* **95** 012125
[3] Zhao W L, Wang J, Wang X and Tong P 2019 *Phys. Rev. E* **99** 042201
[4] Ashida Y, Gong Z and Ueda M 2020 *Adv. Phys.* **69** 249
[5] Bergholtz E J, Budich J C and Kunst F K 2021 *Rev. Mod. Phys.* **93** 015005
[6] Tang J, Hu Z, Zeng Z Y, Xiao J, Li L, Chen Y, Chen A X and Luo X 2022 *J. Phys. B: At. Mol. Opt. Phys.* **55** 245301
[7] Zhang H, Peng M, Xu X W and Jing H 2022 *Chin. Phys. B* **31** 014215
[8] Li Z, Hu X, Xiao J, Chen Y and Luo X 2023 *Phys. Rev. A* **108** 052211
[9] Bender C M and Boettcher S 1998 *Phys. Rev. Lett.* **80** 5243
[10] Kunst F K, Edvardsson E, Budich J C and Bergholtz E J 2018 *Phys. Rev. Lett.* **121** 026808
[11] Jing, H, Özdemir S K, Lü X Y, Zhang J, Yang L and Nori F 2014 *Phys. Rev. Lett.* **113** 053604
[12] Assawaworrarit S, Yu X and Fan S 2017 *Nature* **546** 387
[13] J. Zhang, Peng B, Özdemir Ş K, Pichler K, Krimer D O, Zhao G, Nori F, Liu Y, Rotter S and Yang L 2018 *Nat. Photon.* **12** 479
[14] Song J, Yang F, Guo Z, Wu X, Zhu K, Jiang J, Sun Y, Li Y, Jiang H and Chen H 2021 *Phys. Rev. Appl.* **15** 014009
[15] Huang Y, Yin Z Q and Yang W L 2016 *Phys. Rev. A* **94** 022302
[16] Xiao L, Zhan X, Bian Z H, Wang K K, Zhang X, Wang X P, Li J, Mochizuki K, Kim D, Kawakami N, Yi W, Obuse H, Sanders B C and Xue P 2017 *Nat. Phys.* **13** 1117
[17] Wu Y, Liu W, Geng J, Song X, Ye X, Duan C K, Rong X and Du J 2019 *Science* **364** 878
[18] Li J, Harter A K, Liu J, Melo L de, Joglekar Y N and Luo L 2019 *Nat. Commun.* **10** 855

[19] Naghiloo M, Abbasi M, Joglekar Y N and Murch K W 2019 *Nat. Phys.* **15** 1232
[20] Li L, Lee C H and Gong J 2020 *Phys. Rev. Lett.* **124** 250402
[21] Yu S, Meng Y, Tang J S, Xu X Y, Wang Y T, Yin P, Ke Z J, Liu W, Li Z P, Yang Y Z, Chen G, Han Y J, Li C F and Guo G C 2020 *Phys. Rev. Lett.* **125** 240506
[22] Wang W C, Zhou Y L, Zhang H L, Zhang J, Zhang M C, Xie Y, Wu C W, Chen T, Ou B Q, Wu W, Jing H and Chen P X 2021 *Phys. Rev. A* **103** L020201
[23] Ding L, Shi K, Zhang Q, Shen D, Zhang X and Zhang W 2021 *Phys. Rev. Lett.* **126** 083604
[24] Zhang J W, Zhang J Q, Ding G Y, Li J C, Bu J T, Wang B, Yan L L, Su S L, Chen L, Nori F, Özdemir Ş, K, Zhou F, Jing H and Feng M 2022 *Nat. Commun.* **13** 6225
[25] Klauck F, Teuber L, Ornigotti M, Heinrich M, Scheel S and Szameit A 2019 *Nat. Photon.* **13** 883
[26] Liu W, Wu Y, Duan C K, Rong X and Du J 2021 *Phys. Rev. Lett.* **126** 170506
[27] Abbasi M, Chen W, Naghiloo M, Joglekar Y N and Murch K W 2022 *Phys. Rev. Lett.* **128** 160401
[28] Miri M A and Alù A 2019 *Science* **363** eaar7709
[29] Minganti F, Miranowicz A, Chhajlany R W and Nori F 2019 *Phys. Rev. A* **100** 062131
[30] Chen W, Abbasi M, Ha B, Erdamar S,Joglekar Y N and Murch K W 2022 *Phys. Rev. Lett.* **128** 110402
[31] Peng B, Özdemir Ş K, Rotter S, Yilmaz H, Liertzer M, Monifi F, Bender C M, Nori F and Yang L 2014 *Science* **346** 328
[32] Lin Z, Ramezani H, Eichelkraut T, Kottos T, Cao H and Christodoulides D N 2011 *Phys. Rev. Lett.* **106** 213901
[33] Shu X, Li A, Hu G, Wang J, Alù A and Chen L 2022 *Nat. Commun.* **13** 2123
[34] Schumer A, Liu Y, Leshin J, Ding L, Alahmadi Y, Hassan A U, Nasari H, Rotter S, Christodoulides D N, LiKamWa P and Khajavikhan M 2022 *Science* **375** 884
[35] Gopalakrishnan S and Gullans M J 2021 *Phys. Rev. Lett.* **126** 170503
[36] Turkeshi X and Schiró M 2023 *Phys. Rev. B* **107** L020403
[37] Li Z Z, Chen W, Abbasi M, Murch K W and Whaley K B 2023 *Phys. Rev. Lett.* **131** 100202
[38] Zhang J, Zhou Y L, Zuo Y L, Chen P X, Jing H and Kuang L M 2023 arXiv:2305.19034v1 [quant-ph]
[39] Zhang Y X, Zhang Z T, Wei X Z, Liang B L, Mei F and Yang Z S 2023 arXiv:2308.16079v1 [quant-ph]
[40] Cao P C and Zhu X F 2021 *Chin. Phys. B* **30** 030505
[41] Ding P Z and Yi W 2022 *Chin. Phys. B* **31** 010309
[42] Bu J T, Zhang J Q, Ding G Y, Li J C, Zhang J W, Wang B, Ding W Q, Yuan W F, Chen L, Özdemir Ş K, Zhou F, Jing H and Feng M 2023 *Phys. Rev. Lett.* **130** 110402
[43] Chen S L, Chen G Y and Chen Y N 2014 *Phys. Rev. A* **90** 054301
[44] Kumar A, Murch K W and Joglekar Y N 2022 *Phys. Rev. A* **105** 012422
[45] Gong Z, Ashida Y, Kawabata K, Takasan K, Higashikawa S and Ueda M 2018 *Phys. Rev. X* **8** 031079
[46] Huber J, Kirton P, Rotter S and Rabl P 2020 *SciPost Phys.* **9** 052
[47] Kawabata K, Shiozaki K and Ryu S 2021 *Phys. Rev. Lett.* **126** 216405
[48] Roccati F, Lorenzo S, Palma G M, Landi G T, Brunelli M and Ciccarello F 2021 *Quantum Sci. Technol.* **6** 025005
[49] Hu Z, Zeng Z Y, Tang J and Luo X B 2022 *Acta Phys. Sin.* **71** 074207 (in Chinese)
[50] Li J Z, Zhao W L and Liu J 2023 *Phys. Rev. A* **107** 032208
[51] Chen W, Abbasi M, Joglekar Y N and Murch K W 2021 *Phys. Rev. Lett.* **127** 140504
[52] Bennett C H, Bernstein H J, Popescu S and Schumacher B 1996 *Phys. Rev. A* **53** 2046
[53] Wootters W K 1998 *Phys. Rev. Lett.* **80** 2245
[54] Fang Y L, Zhao J L, Chen D X, Zhou Y H, Zhang Y, Wu Q C, Yang C P and Nori F 2022 *Phys. Rev. Research* **4** 033022